

# Rapid inward migration of planets formed by gravitational instability

Clément Baruteau<sup>1,2\*</sup>, Farzana Meru<sup>3,4</sup> and Sijme-Jan Paardekooper<sup>1</sup>

<sup>1</sup>*DAMTP, University of Cambridge, Wilberforce Road, Cambridge CB3 0WA, UK*

<sup>2</sup>*Department of Astronomy and Astrophysics, University of California, Santa Cruz, CA 95064, USA*

<sup>3</sup>*School of Physics, University of Exeter, Stocker Road, Exeter, EX4 4QL, UK*

<sup>4</sup>*Institut für Astronomie und Astrophysik, Universität Tübingen, Auf der Morgenstelle 10, 72076 Tübingen, Germany*

Accepted 2011 June 1. Received 2011 May 30; in original form 2011 March 25

## ABSTRACT

The observation of massive exoplanets at large separation ( $\gtrsim 10$  AU) from their host star, like in the HR 8799 system, challenges theories of planet formation. A possible formation mechanism involves the fragmentation of massive self-gravitating discs into clumps. While the conditions for fragmentation have been extensively studied, little is known of the subsequent evolution of these giant planet embryos, in particular their expected orbital migration. Assuming a single planet has formed by fragmentation, we investigate its interaction with the gravitoturbulent disc it is embedded in. Two-dimensional hydrodynamical simulations are used with a simple prescription for the disc cooling. A steady gravitoturbulent disc is first set up, after which simulations are restarted including a planet with a range of masses approximately equal to the clump's initial mass expected in fragmenting discs. Planets rapidly migrate inwards, despite the stochastic kicks due to the turbulent density fluctuations. We show that the migration timescale is essentially that of type I migration, with the planets having no time to open a gap. In discs with aspect ratio  $\sim 0.1$  at their forming location, planets with a mass comparable to, or larger than Jupiter's can migrate in as short as  $10^4$  years, that is, about 10 orbits at 100 AU. Massive planets formed at large separation from their star by gravitational instability are thus unlikely to stay in place, and should rapidly migrate towards the inner parts of protoplanetary discs, regardless of the planet mass.

**Key words:** accretion, accretion discs — turbulence — methods: numerical — planetary systems: formation — planetary systems: protoplanetary discs

## 1 INTRODUCTION

The large majority of exoplanets have been discovered by the radial velocity and transiting techniques. Recent progress in the adaptive optics technique has revealed about 20 exoplanets by direct imaging. Since the latter requires a high brightness contrast between the planet and the parent star, massive planets have been observed at separations  $\gtrsim 10$  AU (e.g., Kalas et al. 2008; Marois et al. 2008; Lagrange et al. 2010; Lafrenière et al. 2010; Marois et al. 2010). One such example is the HR 8799 system (Marois et al. 2010), which comprises four planets with masses evaluated between 7 and 10 Jupiter-mass, and estimated separations of 14, 24, 38 and 68 AU, respectively.

How can the large orbital separations of such massive planets be explained? With the standard core accretion formation scenario (e.g., Safronov 1969; Mizuno 1980; Pollack et al. 1996; Ida & Lin 2004), it is difficult to form Jupiter-like planets in isolation further than  $\sim 10$  AU from a Sun-like star. Still, the formation of a first gap-opening planet close to the snow line (Ida & Lin 2004) could pave the way for the formation of a second-generation planet at the outer edge of the first planet's gap (Bryden et al. 2000; Thommes 2005; Ida & Lin 2008). Provided that the second planet opens a gap, its outer edge could also trigger the formation of a third-generation planet. Subsequent planet formation could proceed as a sequence, as long as there are enough planetesimals and gas left.

The tidal interaction between a planet and its nascent protoplanetary disc alters the planet's

\* E-mail: C.Baruteau@damtp.cam.ac.uk

semi-major axis, causing its orbital migration (Goldreich & Tremaine 1980). Assuming the central object is a Sun-like star, a planet typically more massive than Saturn opens a gap around its orbit and generally migrates inwards. It is thus unlikely that a massive planet formed through the core-accretion scenario within  $\sim 10$  AU of its host star could migrate to a separation as large as 100 AU. A notable exception was proposed by Crida et al. (2009), who showed that the tidal interaction between a pair of resonant massive planets embedded in a common gap, and their protoplanetary disc, could drive both planets to orbital separations much larger than that of their birth place, providing some specific conditions on the planets mass ratio and on the disc's turbulent viscosity.

Another in-situ formation scenario is based on the gravitational instability (e.g., Cameron 1978; Boss 1997). It involves early-stage protoplanetary discs, which are massive enough for its self-gravity to play a part in its evolution. The probability that discs form fragments is described by two dimensionless parameters. One is the Toomre Q-parameter,  $Q = c_s \kappa / \pi G \Sigma$ , where  $G$  is the gravitational constant,  $c_s$  and  $\Sigma$  denote the disc's sound speed and surface mass density, and  $\kappa$  is the epicyclic frequency. For Keplerian discs,  $\kappa$  approximately equals the angular frequency  $\Omega$ . Toomre (1964) showed that, for an infinitesimally thin disc to fragment,  $Q \lesssim 1$ . The second parameter describing the stability of a self-gravitating disc is the disc's cooling timescale in units of the orbital timescale,  $\beta = t_{\text{cool}} \Omega$ , where  $t_{\text{cool}} = e(de/dt)^{-1}$  is the cooling timescale and  $e$  the disc's thermal energy density (Gammie 2001). The critical value of the cooling parameter  $\beta$ , below which fragmentation will occur if  $Q \lesssim 1$ , depends on the disc's adiabatic index (Rice et al. 2005), and on the local disc to primary mass ratio (Meru & Bate 2011b). Its exact value is currently somewhat uncertain as Meru & Bate (2011a) have recently shown that previous simulations that determined this critical value were unresolved. However, current simulations show that the critical value for  $\beta$  could be in the range 3 – 18 (Gammie 2001; Rice et al. 2005; Meru & Bate 2011a,b).

The vast majority of studies of planet formation by gravitational instability have focused on the conditions to fragment discs into bound objects. It is thought to operate at separations larger than 30 – 50 AU from the central (Sun-like) star (e.g., Rafikov 2005; Matzner & Levin 2005; Stamatellos & Whitworth 2008). However, little is known of the evolution of these objects, in particular their expected migration resulting from the gravitational interaction with the gravitoturbulent disc they are embedded in. A few numerical studies have observed that clumps could drift inwards (e.g., Mayer et al. 2002; Boss 2005; Cha & Nayakshin 2010), and some of them have focused on the early phases of disc formation and evolution following the collapse from the prestellar core stage (Vorobyov & Basu 2006, 2010a,b; Machida et al. 2011). As these giant planet embryos migrate inwards, they may become tidally disrupted (when their radius becomes comparable to the clump's Hill radius), thereby delivering a variety of planets in the inner parts of protoplanetary discs (Nayakshin 2010).

In this paper, we examine the orbital evolution of

a single planet embedded in its nascent gravitoturbulent disc, following the assumption that the planet has formed by gravitational instability. We show that the planet migrates inwards in a timescale very similar to that of type I migration (Paardekooper & Papaloizou 2009) in the absence of turbulence. Our physical and numerical models are described in Section 2. In Section 3, we present our results of simulations. Conclusions and future directions are drawn in Section 4.

## 2 MODEL

We investigate the tidal interaction between a massive planet and the protoplanetary disc it formed in through the gravitational instability scenario. Once a gaseous clump has formed by fragmentation, it contracts until  $H_2$  dissociation occurs, causing a rapid collapse of the clump down to planetary sizes. Our study does not address the formation of the planet, and we consider the clump and the planet as one object. In the following, our system of interest (clump and planet) is referred to as the planet. Our study focuses on its migration driven by the interaction with the disc, following the assumption that the planet has formed by gravitational instability. As described below, our approach is to first set up a steady state gravitoturbulent disc, then include a single planet and follow its orbital migration.

The disc's properties after fragmentation are poorly constrained. They depend on how many clumps form, and how massive they are. In our study, we assume that the disc properties (density, temperature) are virtually unchanged by the fragmentation stage. In particular, we assume that the disc remains gravitoturbulent. This assumption is motivated by the findings of previous numerical studies on disc fragmentation (e.g., Meru & Bate 2011b), where the images of the discs show similar structures after the formation of a clump.

We carried out two-dimensional (2D) hydrodynamical simulations using the grid-based, staggered-mesh code FARGO<sup>1</sup> (Masset 2000), for which a self-gravity solver based on fast Fourier transforms was presented in Baruteau & Masset (2008b). When calculating the self-gravitating acceleration, all mass is assumed to be confined to the disc midplane (the razor-thin disc approximation). The thermal energy density  $e$  satisfies the equation

$$\frac{\partial e}{\partial t} + \nabla \cdot (e \mathbf{v}) = -(\gamma - 1)e \nabla \cdot \mathbf{v} + Q_{\text{bulk}}^+ - \frac{e}{\tau_{\text{cool}}}, \quad (1)$$

where  $\mathbf{v}$  denotes the gas velocity, and  $\gamma$  is the adiabatic index (its value can be mapped to a three-dimensional adiabatic index, see Gammie 2001, and references therein). In Eq. (1), the cooling timescale  $\tau_{\text{cool}} = \beta \Omega^{-1}$ , with  $\beta$  taken to be constant, and the heating source term  $Q_{\text{bulk}}^+$  is provided by artificial viscous heating at shocks arising from the gravitoturbulence. A von Neumann-Richtmyer artificial bulk viscosity is used, as

<sup>1</sup> See [fargo.in2p3.fr](http://fargo.in2p3.fr).

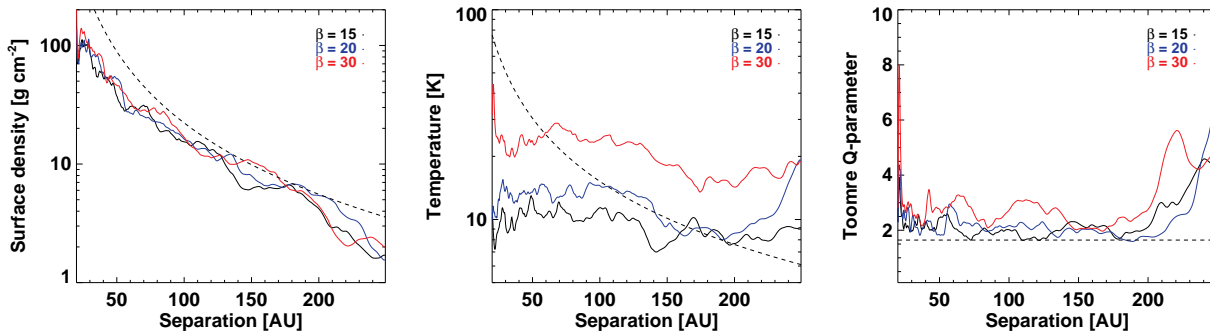


**Figure 1.** Azimuthally-averaged surface density (left panel), temperature (middle panel), and Toomre  $Q$ -parameter (right panel) obtained at 30 orbits for our three values of  $\beta = t_{\text{cool}} \Omega$  (solid curves). The azimuthal average of  $Q$  was calculated as  $\langle c_s \rangle \langle \Omega \rangle / \pi G \langle \Sigma \rangle$ , where  $\langle . \rangle$  stands for the azimuthal average. Dashed curves depict the initial value of each quantity.

described in Stone & Norman (1992), where the coefficient  $C_2$  is taken equal to 1.4 ( $C_2$  measures the number of zones over which a shock is spread over by the artificial viscosity). Providing angular momentum transport driven by gravitoturbulence occurs locally, which is not necessarily the case (Balbus & Papaloizou 1999; Cossins et al. 2009), the alpha parameter associated with the angular momentum flux density is given by (Gammie 2001)

$$\alpha = \frac{4}{9} \frac{1}{\gamma(\gamma - 1)\beta}, \quad (2)$$

which indicates that varying  $\beta$  is equivalent to varying the viscous stress in the disc. Preliminary calculations with our fiducial setup (initial profiles and grid's resolution are described below) showed that the critical value of  $\beta$  below which fragmentation occurs ranges from 10 to 15. Since we require the disc to be in a gravitoturbulent state, but we do not require further fragmentation so as to focus on the migration of a single planet, we simulated three disc models with  $\beta = 15, 20$  and 30.

Each of our three models initially comprises a  $0.4M_{\odot}$  2D disc around a star of fixed mass  $M_{\star} = 1M_{\odot}$ , and spanning a radial range  $20 < r < 250$  AU. (As will be shown in Section 3.1, the disc mass rapidly decreases to about  $0.2 - 0.25M_{\odot}$  after 30 orbits at 100 AU). The initial surface mass density decreases as  $r^{-2}$ , and it equals  $\approx 20 \text{ g cm}^{-2}$  at 100 AU. The initial disc's temperature is  $\approx 15 \text{ K}$  at 100 AU, and it decreases as  $r^{-1}$  (we assume a mean-molecular weight  $\mu = 2.4$  and an adiabatic index  $\gamma = 5/3$ ). This corresponds to setting the initial disc aspect ratio  $h$  (pressure scale height to radius ratio  $H/r$ ) equal to 0.1 at 100 AU. The disc's initial Toomre  $Q$ -parameter is thus uniform, equal to 2. A small level ( $\sim 0.1\%$ ) of white noise is added initially to break the disc's axisymmetry. Here and in the following, disc and planet quantities are expressed in physical units. Since our simulations are scale-free, all the results presented throughout this paper can be easily rescaled by using different units of mass, length and temperature.

In all our simulations, the grid is covered with 512 and 1536 cells along the radial and azimuthal directions, respectively. A logarithmic spacing is used along the radial direction, as required by the self-gravity module in

FARGO. Grid cells are approximately square, and the initial pressure scale height is resolved by about 20 cells along each direction. The radial and azimuthal components of the self-gravitating acceleration are smoothed over a softening length,  $\varepsilon_{\text{sg}}$ . We take  $\varepsilon_{\text{sg}} = 3 \times 10^{-4} r$  throughout this study, which is a factor  $3 \times 10^{-3}$  times the initial pressure scale height. The influence of a large  $\varepsilon_{\text{sg}}$ , which can be seen as a crude treatment of the effects of finite thickness, will be examined in Sect. 3.2.4, where we find that the choice for  $\varepsilon_{\text{sg}}$  does not significantly alter the orbital evolution of a planet embedded in a gravitoturbulent disc. Outflow boundary conditions are used at the grid's inner and outer edges. Hydrodynamical equations are solved in the frame centred onto the central star. Since a non-inertial frame of reference is adopted, the indirect terms in the expression for the disc's gravitational potential are included.

### 3 RESULTS OF HYDRODYNAMICAL SIMULATIONS

Our numerical simulations were carried out in two steps. In a first step, a gravitoturbulent disc model was set up, whose properties are described in Section 3.1. We then restarted the simulations, including planets of several masses, and following the time-evolution of their orbital separation. The results of the restart simulations are presented in Section 3.2. Further investigation on the impact of the disc's temperature follows in Section 3.3.

#### 3.1 Gravitoturbulent stage

We describe in this section the results of our three disc models with cooling parameters  $\beta = 15, 20$  and 30. The absence of heating source initially leads to decrease the disc's temperature, and thus the Toomre  $Q$ -parameter, until gravitoturbulence sets in. As both the initial  $Q$ -profile and  $\beta$  are taken to be uniform (the cooling timescale thus scales proportional to the orbital timescale), gravitoturbulence progressively develops through the disc, starting from the inner edge. After a few orbits at the disc's outer edge, a thermal quasi-equilibrium is reached over the whole disc, where cooling

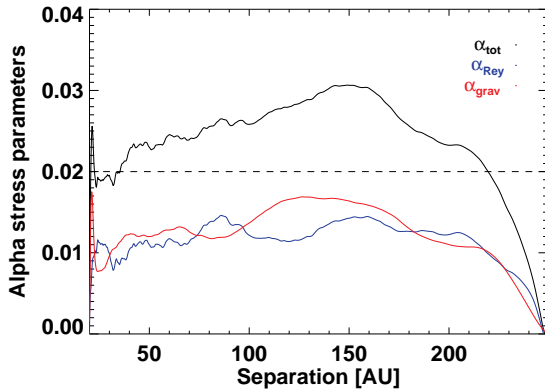


**Figure 2.** Gravitational, Reynolds and total alpha parameters, azimuthally- and time-averaged from 30 to 60 orbits at 100 AU (that is, over  $\approx 8$  orbits at 250 AU, the location of the disc’s outer edge). Results are displayed for the disc model with cooling parameter  $\beta = 20$ . The dashed curve shows the total alpha parameter expected from viscous transport theory, given by Eq. (2).

is approximately balanced by shock heating due to gravitoturbulence.

The disc’s initial surface density that we assume does not correspond to a mechanical equilibrium with the gravitoturbulent stress. The disc therefore adjusts both its surface density and temperature profiles to satisfy a mechanical equilibrium along with a uniform Toomre- $Q$  profile. This is illustrated in Fig. 1, where the azimuthally-averaged surface mass density, temperature, and Toomre  $Q$ -parameter are depicted at 30 orbits at 100 AU. Their initial value is shown with a dashed curve. In this quasi-steady state, the surface density profile decreases approximately as  $r^{-3/2}$ , and the disc’s temperature is almost uniform, as is the Toomre  $Q$ -parameter. We comment that the high initial disc mass ( $0.4M_{\odot}$ ) promotes global modes that, along with the outflow boundary condition at the grid’s inner edge, lead to a rapid decrease in the disc mass. After 30 orbits at 100 AU, the latter ranges from  $0.21M_{\odot}$  to  $0.24M_{\odot}$  for  $\beta$  increasing from 15 to 30. The rate at which the disc mass decreases is maximum at the onset of gravitoturbulence, and then declines (but does not vanish) as a quasi-steady state is attained.

The alpha parameters associated with the Reynolds and gravitational turbulent stresses are denoted by  $\alpha_{\text{Rey}}$  and  $\alpha_{\text{sg}}$ , respectively. Details of their calculation in a 2D disc model are given in the Appendix. Fig. 2 displays the azimuthally- and time-averaged radial profiles of  $\alpha_{\text{Rey}}$ ,  $\alpha_{\text{sg}}$  and of  $\alpha_{\text{tot}} = \alpha_{\text{sg}} + \alpha_{\text{Rey}}$ . Time average is done from 30 to 60 orbits at 100 AU (that is, over  $\approx 8$  orbits at the grid’s outer edge). Results are shown for  $\beta = 20$ . We note that  $\alpha_{\text{sg}}$  and  $\alpha_{\text{Rey}}$  take very similar values over the whole disc. The same behavior was obtained by Gammie (2001) with 2D local shearing-sheet calculations. The decrease in both  $\alpha_{\text{sg}}$  and  $\alpha_{\text{Rey}}$  at large ( $\gtrsim 200$  AU) separation is most probably due to the decreasing grid’s resolution, as a logarithmic spacing is used along the radial direction. We comment that  $\alpha_{\text{tot}}$  is locally up to 50% larger

than the value expected from viscous (local) transport theory, given by Eq. (2). The difference is probably due to our large disc mass ( $\gtrsim 0.2M_{\star}$ ) and large aspect ratio ( $h \sim 0.1$ ), which tend to foster global transport<sup>2</sup> of angular momentum (e.g., Lodato & Rice 2004). Although not shown here, very similar results were obtained for  $\beta = 15$  and  $\beta = 30$ .

Finite resolution effects (numerical diffusion) leads to a negligible transport of angular momentum compared to gravitoturbulence (see e.g., Lin & Papaloizou 2010, who estimated the numerical “alpha viscosity” in the FARGO code to be  $\lesssim 10^{-5}$  for a number of grid cells similar to ours). Artificial bulk viscosity most likely leads to a small, if not negligible transport of angular momentum compared to gravitoturbulence, but note that it is unclear how its contribution can be isolated in our simulations. We point out that if artificial bulk viscosity induced a net transport of angular momentum on average, it would lead to a discrepancy between the value of  $\alpha_{\text{sg}} + \alpha_{\text{Rey}}$  measured in local, steady-state disc models and the alpha value given in Eq. (2). Gammie (2001) carried out 2D local shearing-sheet simulations of gravitoturbulent disc models using the ZEUS code, which is very similar to the FARGO code. In particular, both codes use the same prescription for the artificial bulk viscosity. He found that  $\alpha_{\text{sg}} + \alpha_{\text{Rey}}$  agrees with the value given by the expression in Eq. (2) to within  $\sim 10\%$ , which shows that artificial bulk viscosity should lead to a small transport of angular momentum compared to gravitoturbulence. Also, although not shown here, we have checked that increasing the amount of artificial bulk viscosity (the coefficient  $C_2$  in Stone & Norman 1992) by a factor of 3 leads to a negligible change in the values of  $\alpha_{\text{Rey}}$  and  $\alpha_{\text{sg}}$ .

### 3.2 Restart with an embedded planet

We restarted the simulations of Section 3.1 at 30 orbits, including a single planet at 100 AU. The disc’s temperature and surface mass density at this location are close to their initial value for our three values of  $\beta$  (see Fig. 1). Note in particular that the disc aspect ratio at the planet’s initial location is  $\approx 0.1$ . Akin to the clump’s contraction timescale, the final mass of planets formed by gravitational instability is uncertain (e.g., Boley et al. 2010; Helled & Bodenheimer 2011), and may substantially differ from the clump’s initial mass. The latter is estimated by Boley et al. (2010) as  $\sim h_p^3 M_{\star}$  for  $Q \sim 1.5$ , with  $h_p$  the disc aspect ratio at the clump’s forming location. This estimate of the clump’s initial mass, which is based on the fragmentation of spiral arms, is typically a factor 5 – 10 smaller than the Toomre mass (see Boley et al. 2010, their figure 1, and references therein). We considered three planet masses corresponding to a

<sup>2</sup> Similar gravitoturbulent disc models, but with reduced aspect ratio in a steady state, have been simulated by Paardekooper et al. (2011) with the same hydrodynamical code and similar grid resolution. Using the same method to calculate the stresses as described in the appendix, they find an averaged value of  $\alpha_{\text{tot}}$  in very good agreement with the value given in Eq. (2).

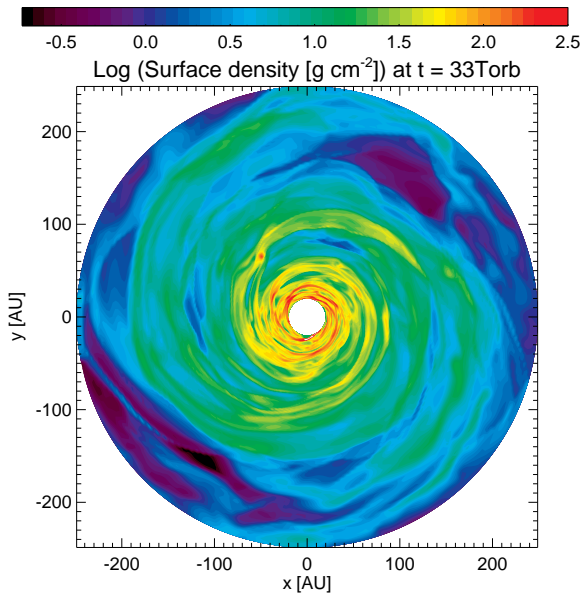


**Figure 3.** Contours of the disc’s surface density obtained in a restart simulation with  $\beta = 30$ , where a Jupiter-mass planet has been introduced at 100 AU. Results are displayed three orbits after the restart time. The planet is now located at about 60 AU from the central star (at  $x \sim -60$  AU,  $y \sim 60$  AU).

planet to primary mass ratio  $q = M_p/M_*$  around  $h_p^3$ : a Saturn-mass planet ( $q = 3 \times 10^{-4}$ ,  $q/h_p^3 \sim 0.3$ ), a Jupiter-mass planet ( $q = 10^{-3}$ ,  $q/h_p^3 \sim 1$ ), and a 5 Jupiter-mass planet ( $q = 5 \times 10^{-3}$ ,  $q/h_p^3 \sim 5$ ). The planets gravitational potential is softened over a smoothing length  $\varepsilon = 3 \times 10^{-2} r_p$ , with  $r_p$  the planet’s orbital separation, and it takes its maximum value at the restart time (we do not gradually ramp up the planet’s mass). We will show in Section 3.2.4 that our results are not altered by a more gentle introduction of the planet’s potential in the disc over a dynamical timescale, the typical formation timescale of a clump. We comment that in self-gravitating discs, the mass that is relevant for disc–planet interactions is the mass of the planet and of the gas envelope surrounding it. Although for simplicity the planet’s mass is fixed, gas can be accreted onto its envelope (circumplanetary disc), thereby contributing to increasing the effective planet’s mass. Note however that this accretion rate is probably not realistic due to our simple prescription for the disc cooling. Since the disc is fully self-gravitating, the calculation of the force exerted on the planet takes all the disc into account, it does not partly exclude the planet’s Hill radius (Crida et al. 2009).

Fig. 3 displays the surface density obtained for the disc model with  $\beta = 30$ , perturbed by a Jupiter-mass planet. Density contours are shown only three orbits after the restart, the planet is now located at  $\approx 60$  AU from the central object. The density perturbation due to the planet’s potential is comparable to the turbulent density perturbations. This similarity stresses that the magnitude of the stochastic torque acting on the planet can be similar to that of the disc–planet tidal torque obtained in the absence of turbulence (e.g., Nelson & Papaloizou

2004; Baruteau & Lin 2010). In such turbulent configurations, the migration timescale must be evaluated in a statistical way, by running several simulations. For each planet mass and each value of  $\beta$ , we performed a suite of eight simulations, varying the planet’s azimuth at restart as  $\varphi_p = \pi/4 \times i$ ,  $i \in [0 - 7]$  (that is, independently of the disc’s density structure at restart). The migration timescales obtained for these series of runs are presented in Section 3.2.1. The impact of stochastic density fluctuations is described in Section 3.2.2. A comparison with predictions of laminar disc models follows in Section 3.2.3, and a brief discussion on the impact of numerics is given in Section 3.2.4.

### 3.2.1 Migration timescale

The time evolution of the planets’ orbital separation is displayed in Fig. 4. Planet mass increases from left to right, and the cooling parameter  $\beta$  increases from top to bottom. In all panels, time is expressed in years (bottom x-axis), and in orbital periods at 100 AU (top x-axis). Results are shown for the eight evenly-spaced values of the planet’s azimuth  $\varphi_p$  at restart (increases with increasing color’s wavelength).

The net trend coming out of our results is that, in spite of the stochastic kicks triggered by turbulence, planets migrate inwards very rapidly. Averaging over  $\varphi_p$  and  $\beta$ , the migration timescale (defined as the time to migrate from 100 AU to 20 AU, the location of the grid’s inner edge) is typically as short as 3 orbits for the 5 Jupiter-mass planet, 6 orbits for the Jupiter-mass planet, and about 8 orbits for the Saturn-mass planet. In addition, at fixed  $\beta$ , the amplitude of stochastic kicks increases with decreasing planet mass, and so does the spread in the migration timescale. Both results may be qualitatively interpreted as follows. The torque exerted by the disc on the planet may be decomposed as a background tidal torque, plus a stochastic torque due to turbulent fluctuations. In the mass regime that we consider ( $q/h_p^3 \sim 1$ ), the amplitude of the tidal torque should increase with increasing planet mass. However, like in discs with turbulence driven by the magneto-rotational instability, it is unclear if the value of the tidal torque is similar to that predicted in laminar disc models, in the absence of turbulence (Nelson & Papaloizou 2004). A detailed comparison with results of laminar disc models will be presented in Section 3.2.3. The standard deviation of the stochastic torque’s distribution is primarily controlled by  $\alpha_{\text{tot}}$ , and therefore by the cooling parameter  $\beta$  (see Eq. 2). For a given  $\beta$ , the smaller the planet mass, the smaller the tidal torque to stochastic torque ratio, the more sensitive the planet is to stochastic kicks, and therefore the larger the spread in the migration timescale. In the same vein, at fixed planet mass, the spread in the migration timescale should increase with decreasing  $\beta$ . This trend does not clearly show up in Fig. 4, most probably because our minimum and maximum values of  $\beta$  only differ by a factor of 2. Some further insight into the effect of stochastic kicks is given in Section 3.2.2. We finally point out that the disc’s density and temperature profiles do not significantly decrease over the planets migration timescale (for



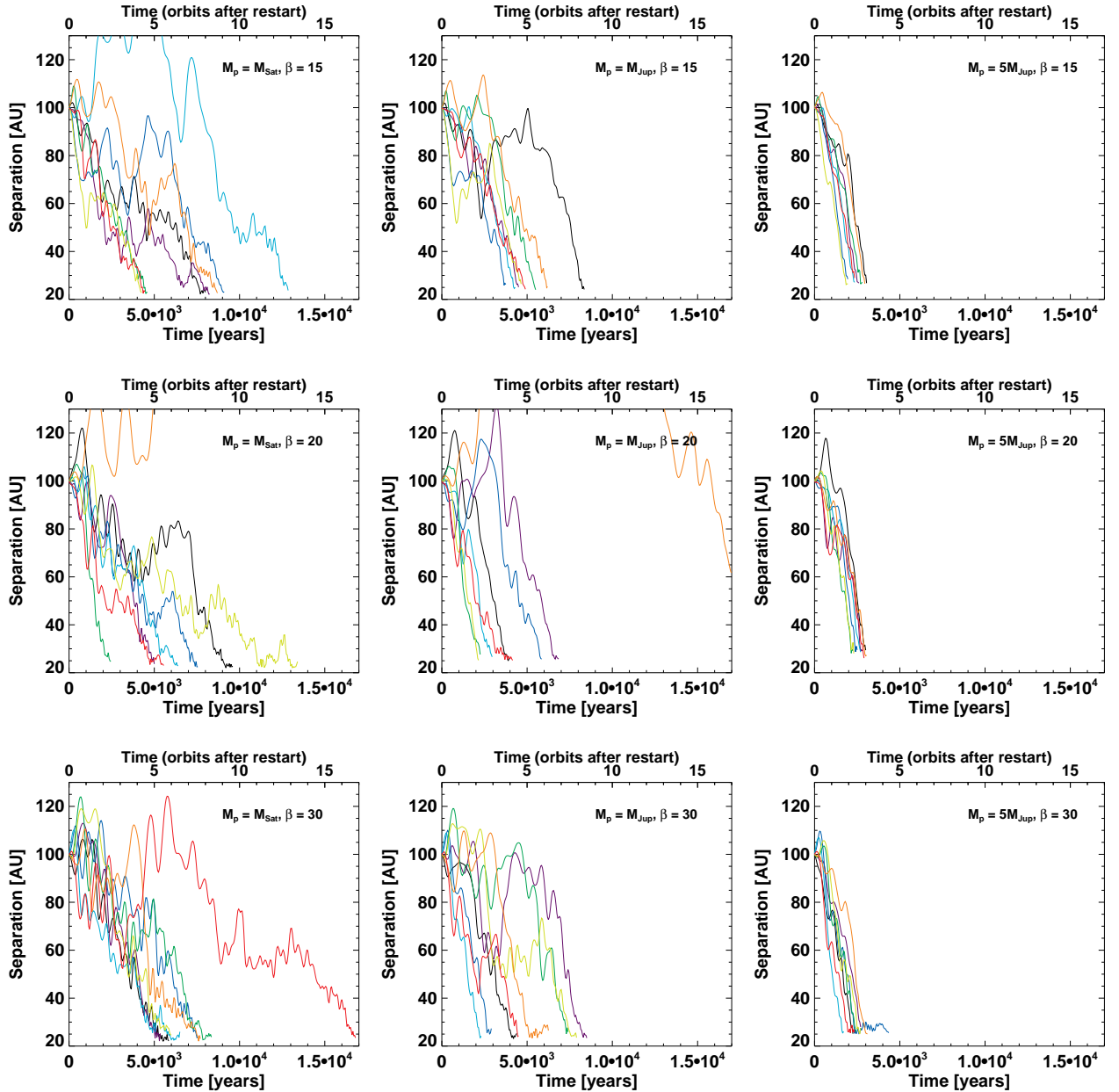


**Figure 4.** Time evolution of the orbital separation of a Saturn-mass planet (left column), a Jupiter-mass planet (middle column), and of a 5 Jupiter-mass planet (right column) in a gravitoturbulent disc with  $\beta = 15$  (top row),  $\beta = 20$  (middle row), and  $\beta = 30$  (bottom row). Time is displayed in years (bottom x-axis), and in orbital periods at 100 AU (top x-axis). Results are obtained for eight evenly-spaced planet's azimuths at restart (azimuth increases with wavelength's color).

the longest simulation with the Saturn-mass planet, the disc's mass decreases by at most 10%).

### 3.2.2 Stochastic kicks

The results of Section 3.2.1 show that planets formed by gravitational instability should rapidly migrate inwards. Even for the Saturn-mass planet, whose mass is smaller than the estimated initial clump's mass (see first paragraph of Section 3.2), inward migration occurs in typically less than 10 orbits. As illustrated in Fig. 4, planet migration in gravitoturbulent discs is not a smooth pro-

cess. Planets may experience large kicks, either inwards or outwards, depending on the local density perturbations they encounter. An example of outward kick is illustrated in Fig. 5, which displays the gas density obtained for the restart simulation with  $\beta = 30$  and the Saturn-mass planet that experiences a significant episode of outward migration in the bottom-left panel of Fig. 4 (red curve). Time increases by 0.1 orbital periods at 100 AU from left to right. In each panel, the planet's location is indicated with a filled black circle.

We first comment that, because the planet's mass is low enough ( $q/h_p^3 \approx 0.3$ ), the wakes it generates are

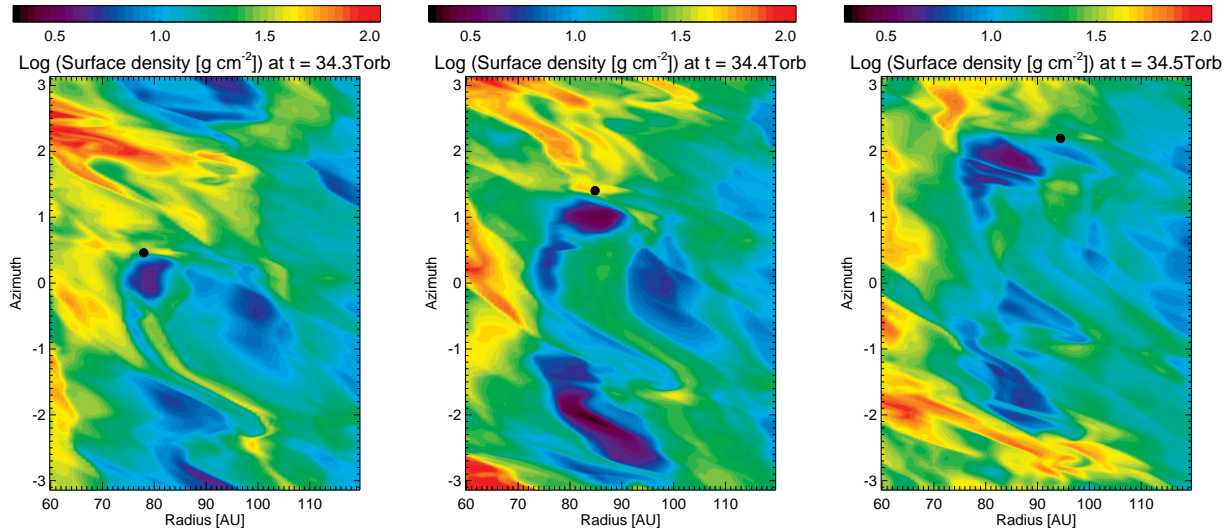


**Figure 5.** Contours of the gas surface density obtained for the restart simulation with  $\beta = 30$ , and the Saturn-mass planet with restart azimuth equal to  $7\pi/4$ . This simulation corresponds to the red curve in the bottom-left panel of Fig. 4, where a significant episode of outward migration occurs from 3 to 6 orbits after restart. Orbital separation is shown on the x-axis, and azimuth on the y-axis. In all panels, the planet's location is depicted with a filled black circle.

invisible, their density contrast being much weaker than that of the turbulent perturbations. In the case depicted in Fig. 5, the planet finds itself with an underdense region behind it, and a (comparatively) overdense region in front of it. This density contrast yields a large, positive coorbital corotation torque that is responsible for the vigorous outward kick experienced by the planet. This kick increases the planet's orbital separation from  $\sim 75$  AU to  $\sim 95$  AU in only 0.2 orbital periods at 100 AU (that is, in 200 years). Similarly, inward kicks are obtained as the planet experiences a negative coorbital corotation torque induced by an underdense region ahead of it, and a (comparatively) overdense region behind it. As is shown for instance in the bottom-left panel of Fig. 4, kicks excite planets epicyclic motion, which is rapidly damped as the underlying disc–planet tidal torque takes over.

The stochastic kicks induced by gravitoturbulence are reminiscent of type III runaway migration. This migration regime relies on the formation of a coorbital mass deficit in the planet's horseshoe region, which takes the form of an asymmetric density structure behind and in front of the planet (Masset & Papaloizou 2003). In massive ( $Q \gtrsim 1$ ) laminar discs with moderate viscosity ( $\alpha$  is a few  $\times 10^{-3}$ ), runaway migration is particularly relevant for planets with  $q \sim h_p^3$  (Masset & Papaloizou 2003), like the planets considered in our study. However, in our model, the disc's turbulent viscosity ( $\alpha_{\text{tot}}$  is a few percent) is too large to allow planets to open a partial dip around their orbit before they reach the disc's inner edge. Thus, planets do not build up a coorbital mass deficit. But, through the density fluctuations it triggers, gravitoturbulence may provide an *effective* mass deficit on each side of the planet, and induce an effective type III migration. However, this effective mass deficit is not coorbital with the planet (as can be seen in Fig. 5), and therefore cannot lead to a runaway. Consequently, the relative fast inward migration that we obtain cannot be attributed to

type III runaway migration. Also, although the planets we consider are massive, their short formation and migration timescales compared to their gap-opening timescale suggests they are subject to type I-like migration instead of type II, perturbed by stochastic kicks. This point will be clarified in Section 3.2.3.

Stochastic kicks provide a source of very fast relative motion between the planet and the disc. Fig. 6 displays the migration speed in units of the local sound speed for the three runs with  $\beta = 30$ , and zero azimuth at restart. The migration rate can be a significant fraction of the local sound speed, and short episodes of supersonic motion are even obtained. We note that the maximum value for the migration speed to sound speed ratio tends to increase with decreasing planet mass, as less massive planets are more sensitive to stochastic kicks.

### 3.2.3 Comparison to laminar disc models

Our results of simulations indicate that the migration of planets embedded in gravitoturbulent discs is driven by both a vigorous (negative) tidal torque, and a (positive or negative) stochastic torque. As the planet mass increases, the former prevails over the latter. In this section, we compare the results of our turbulent disc model with  $\beta = 30$  to those of an equivalent laminar disc model, including the viscous force in the momentum equation. A constant alpha viscosity is used, approximately equal to 1.3%. The comparison is done for the same three planet masses as previously considered. As the initial conditions for the laminar calculations, we take surface density and temperature profiles that fit those of the gravitoturbulent run with  $\beta = 30$  at 30 orbits:  $\Sigma \approx 15 \text{ g cm}^{-2} \times (r/100 \text{ AU})^{-3/2}$ , and  $T \approx 25 \text{ K}$ .

Two series of laminar calculations were carried out: (i) one with an isothermal equation of state, where the imposed (flat) temperature profile remains constant in

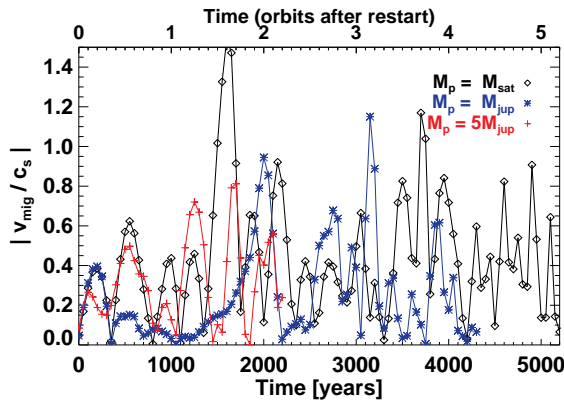


**Figure 6.** Time variation of the (absolute value of the) migration speed, in units of the local sound speed, obtained for the restart simulations with  $\beta = 30$  and zero azimuth at restart. They correspond to the results shown with black curves in the bottom row of Fig. 4. The migration speed is measured as the time derivative of the planet’s orbital separation.

time, and (ii) one with an energy equation with both viscous heating ( $\alpha \approx 1.3\%$ ) and  $\beta$ -cooling ( $\beta = 30$ ). For the latter series, the aforementioned<sup>3</sup> value for  $\alpha$  leads to an initial thermal balance between viscous heating and  $\beta$ -cooling, see Eq. (2).

All laminar calculations include the axisymmetric component of the disc’s self-gravity. This is meant to avoid a large mismatch between the disc’s and the planet’s angular velocities due to the disc gravity, which would yield a spurious shift inwards of all Lindblad resonances, and therefore an artificial acceleration of the inward migration (Baruteau & Masset 2008b). Also, in all laminar runs, the calculation of the force exerted by the disc on the planet excludes the planet’s circumplanetary disc (Crida et al. 2009). All other parameters are otherwise the same as in the gravitoturbulent calculations.

The results with the laminar disc model and an energy equation are depicted in Fig. 7 as solid curves. It takes about 5 orbits for the 5 Jupiter-mass planet to migrate from 100 AU to 50 AU, and about 7 orbits for the Jupiter-mass planet. This corresponds to migration rates  $\sim$  half those of the gravitoturbulent calculations (see bottom row of Fig. 4). Interestingly, the difference in migration rates is larger for the Saturn-mass planet, which drifts from 100 to 60 AU in 20–25 orbits in the laminar run, and (on average) in only 5–6 orbits in the gravitoturbulent run. We note that the migration timescales of the Saturn- and Jupiter-mass planets differ by a factor approximately equal to their mass ratio, as expected in the type I migration regime, wherein the tidal torque encompasses the differential Lindblad torque and the horseshoe drag (Paardekooper & Papaloizou 2009). We comment that it is the large disc aspect ratio ( $h \sim 0.1$ )

<sup>3</sup> As in the case with  $\beta = 20$ , this value of  $\alpha$ , given by viscous transport theory, is slightly smaller than what we measured in the gravitoturbulent disc model ( $\langle \alpha_{\text{tot}} \rangle \approx 1.8\%$ ). We have checked that a higher value of  $\alpha$  does not change our results of laminar calculations, presented below.

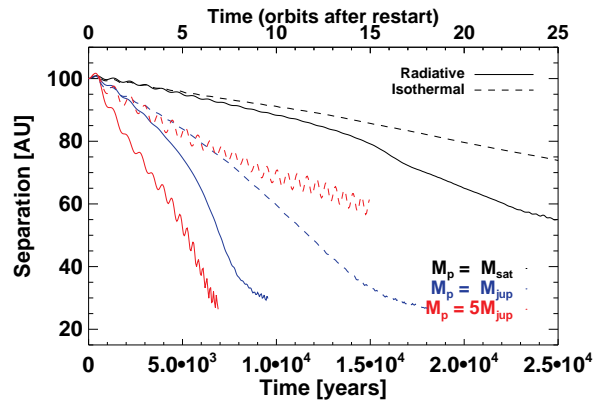


**Figure 7.** Time evolution of the planets’ orbital separation obtained for the laminar disc model with initial profiles of surface density and temperature similar to those of the gravitoturbulent run with  $\beta = 30$  before restart. Solid curves show the results with inclusion of an energy equation (with viscous heating and  $\beta$ -cooling), and dashed curves those with an isothermal equation of state.

that makes the Saturn-mass planet ( $q/h^3 \sim 0.3$ ) and the Jupiter-mass planet ( $q/h^3 \sim 1$ ) relevant to type I migration. The 5 Jupiter-mass planet ( $q/h^3 \sim 5 \gg 1$ ) is, however, more prone to non-linear effects (e.g., Masset et al. 2006). This is presumably why the migration timescales of the Jupiter- and the 5 Jupiter-mass planets do not differ by a factor of their mass ratio. It may seem surprising that the 5 Jupiter-mass planet does not open a gap and migrates in a very short timescale. The gap-opening criterion for a planet on a fixed circular orbit in a laminar viscous disc takes the form (Crida et al. 2006)

$$1.1 \left( \frac{q}{h^3} \right)^{-1/3} + 50 \left( \frac{\alpha}{h} \right) \left( \frac{q}{h^3} \right)^{-1} \lesssim 1, \quad (3)$$

where  $\alpha$  and  $h$  are to be evaluated at the planet’s orbital separation. Although it is unclear to what extent the gap-opening criterion in Eq. (3) may be applied to planets migrating in gravitoturbulent discs, it provides some insight into the fact the planets in our disc models are not expected to clear a gap. Notwithstanding that the large values of  $h$  and  $\alpha$  imply the 5 Jupiter-mass planet does not quite satisfy the above gap-opening criterion (the left-hand side of Eq. (3) typically ranges from 2 to 4 in the disc inner parts), we stress that the vigorous tidal torque exerted by the disc, which is partly due to the large masses of the disc and the planet, conspires to make the planet migrate in a timescale shorter than the timescale required to open a gap (a few libration timescales, which would correspond here to a few tens of orbits). In other words, the 5 Jupiter-mass planet migrates very fast because it has no time to open a gap.

The results of laminar simulations with an isothermal equation of state are overplotted as dashed curves in Fig. 7. The migration rates obtained in this series are smaller than with inclusion of an energy equation. The difference arises from a large, negative horseshoe drag obtained with an energy equation, and driven by a *positive* entropy gradient in our disc model (Baruteau & Masset 2008a; Paardekooper & Papaloizou



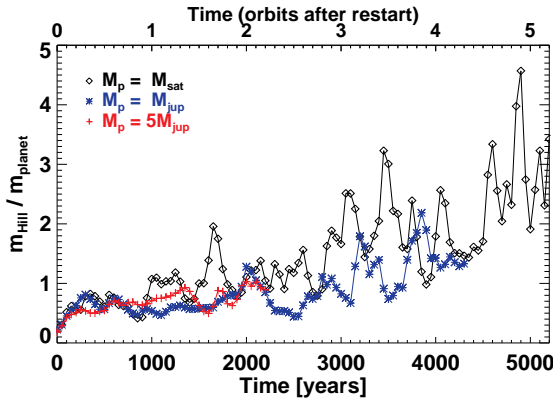


**Figure 8.** Time variation of the mass enclosed in the planet’s Hill radius in units of the planet mass, obtained for the restart simulation with  $\beta = 30$  and zero azimuth at restart. The mass ratio is displayed before the planet crosses the inner edge of the computational domain.

2008; Masset & Casoli 2009; Paardekooper et al. 2010, in our case, the radial profile of the disc entropy scales in proportion to the orbital separation).

Further insight into the impact of the horseshoe drag may be obtained by comparing the migration timescales of our laminar calculations to those predicted by type I migration theory. Note that the predicted migration timescales are inferred from the torque exerted on a planet held on a fixed circular orbit. In the isothermal series, where  $\Sigma \propto r^{-3/2}$  and  $T$  is uniform, the total torque reduces to the differential Lindblad torque. Using Eq. (14) of Paardekooper et al. (2010), we find migration timescales of about 75 and 20 orbits for the Saturn- and Jupiter-mass planets, respectively. This is in good agreement (to within  $\sim 25\%$ ) with our findings (dashed curves in Fig. 7). In the series with the energy equation, the total torque comprises the differential Lindblad torque and the horseshoe drag. Despite the large value of  $\alpha$  in our disc model, the horseshoe drag is found to be fully unsaturated, as the diffusion timescale across the planet’s horseshoe region remains larger than the U-turn timescale (Baruteau & Masset 2008a; Masset & Casoli 2010; Paardekooper et al. 2011). Using Eqs. (14) and (45) of Paardekooper et al. (2010), we now find migration timescales of about 35 and 10 orbits for the Saturn- and Jupiter-mass planets, respectively. This is shorter than what we find (see solid curves in Fig. 7), although still in decent agreement. The difference presumably arises from the large velocity difference between the disc and the planet, which sets asymmetric horseshoe streamlines around the planet’s orbital radius (Masset 2002), an effect that is not taken into account in the horseshoe drag expression of Paardekooper et al. (2010).

We further comment on having a positive entropy gradient in our gravitoturbulent disc model. Let us assume the disc profiles of surface density and temperature scale as  $r^{-\sigma}$  and  $r^{-\varpi}$ , respectively. The disc entropy  $s$ , which we define as  $s \equiv p\Sigma^{-\gamma}$ , where the disc pressure  $p$  verifies the ideal gas equation of state, scales as  $r^{-\xi}$ ,

with  $\xi = \varpi - (\gamma - 1)\sigma$ . As the disc evolves towards a steady state with approximately uniform Toomre- $Q$  profile,  $\xi \sim -3 + \sigma(3 - \gamma)$ . Steady-state gravitoturbulent discs may thus have a globally decreasing profile of entropy only for surface density profiles steeper than  $r^{-9/4}$ , assuming  $\gamma = 5/3$ . Furthermore, for  $\gamma = 5/3$  and our fiducial softening length  $0.3H(r_p)$ , the fully unsaturated horseshoe drag  $\Gamma_{\text{hs}}$  reads (Paardekooper et al. 2010, their Eq. 45)

$$\gamma\Gamma_{\text{hs}}/\Gamma_0 \approx -20.5 + 8.6\sigma, \quad (4)$$

where  $\Gamma_0 = (q/h_p)^2 \Sigma_p r_p^4 \Omega_p^2$ , and all quantities with the subscript  $p$  are to be evaluated at the planet’s location. Eq. (4) shows that, in discs with a uniform Toomre- $Q$  parameter, the horseshoe drag is negative whenever the surface density profile is shallower than  $r^{-2.4}$ , assuming  $\gamma = 5/3$ . The differential Lindblad torque  $\Gamma_L$  can be similarly recast as (Paardekooper et al. 2010, their Eq. 14)

$$\gamma\Gamma_L/\Gamma_0 \approx 3.2 - 4.0\sigma, \quad (5)$$

and the total torque  $\Gamma_{\text{tot}}$  as

$$\gamma\Gamma_{\text{tot}}/\Gamma_0 = -17.3 + 4.6\sigma. \quad (6)$$

Using Eq. (6), the type I migration timescale,  $\tau_I = r_p^2 \Omega_p M_p / 2\Gamma_{\text{tot}}$ , reads

$$\frac{\tau_I}{T_{\text{orb}}} \approx 5.6 \times (3.8 - \sigma)^{-1} \gamma Q_p \left( \frac{q}{h_p^3} \right)^{-1} \left( \frac{h_p}{0.1} \right)^{-2}, \quad (7)$$

where  $T_{\text{orb}}$  stands for the orbital period at the planet’s orbital radius. The estimate in Eq. (7) applies to planets with  $q \sim h_p^3$ , and is approximate, since it is based on the torque expression for a planet on a fixed orbit. As we have already stressed above, the fast relative motion between the disc and planet is likely to affect this estimate. Nevertheless, it indicates that the type I migration of planets formed by fragmentation ( $q \sim h_p^3$ ,  $Q_p \sim 1.5$ ) in discs with moderate aspect ratio ( $h_p \sim 0.1$ ) should typically occur in a few tens of orbits at 100 AU, that is a few  $10^4$  years.

Still, the migration timescales in our gravitoturbulent simulations are a factor of a few shorter than obtained in laminar disc models. In addition to the stochastic kicks due to turbulence, the following two mechanisms may account for the larger migration rates in the gravitoturbulent disc model:

- The non-axisymmetric component of the disc’s self-gravity shifts Lindblad resonances towards the planet’s orbital radius (Pierens & Huré 2005). For discs close to marginal stability, and for our softening parameter ( $\varepsilon/H \sim 0.3$ ), this shift increases the differential Lindblad torque by typically a factor of 2 (Baruteau & Masset 2008b, their Figure 10). Note however that this mechanism has been investigated in laminar disc models. It is therefore not straightforward whether it should behave identically with turbulence. Still, numerical simulations indicate that, on average, the Lindblad torque behaves similarly in laminar and turbulent disc models (Baruteau & Lin 2010, where wave-like turbulence is generated by stochastic forcing of the disc).

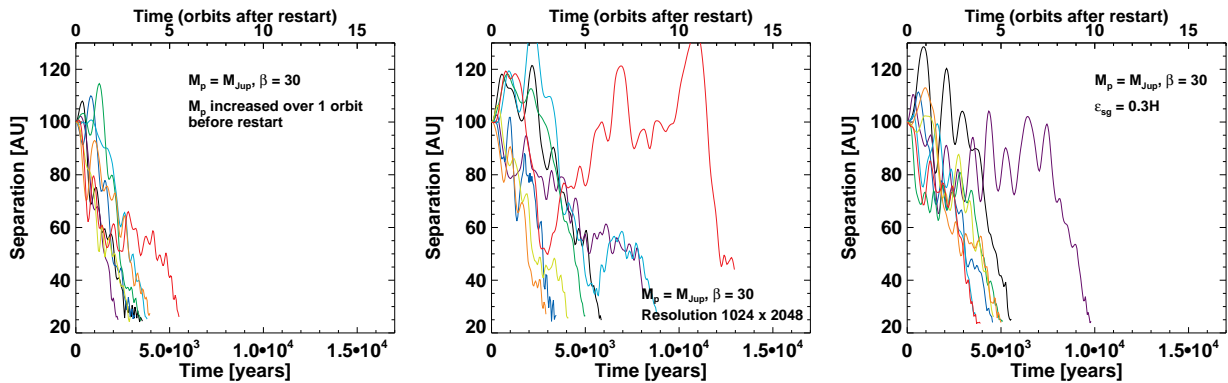


**Figure 9.** Migration of a Jupiter-mass planet in a disc with cooling parameter  $\beta = 30$ . In the left panel, the planet mass is gradually ramped up over one orbit, while the planet is held on a fixed circular orbit. After this first stage (not shown in this panel), the planet is released in the disc. The middle panel shows results at higher resolution ( $1024 \times 2048$ ), and the right panel shows results with increased self-gravitating softening length ( $\varepsilon_{\text{sg}} = 3 \times 10^{-2} r$ ). All three panels should be compared to the mid-bottom panel in Fig. 4, which displays the results of our fiducial setup (no gradual increase of the planet mass, grid resolution is  $512 \times 1536$ , and  $\varepsilon_{\text{sg}} = 3 \times 10^{-4} r$ ).

- In fully self-gravitating discs, the effective mass that dictates the strength of the tidal torque and thus the migration rate not only includes the planet mass, but also the mass of the gas surrounding the planet's location. For massive planets ( $q > h_p^3$ ), the latter corresponds to the planet's circumplanetary disc, which is a fraction of the planet's Hill sphere (Crida et al. 2009). It is unclear what it corresponds to for smaller planets; we speculate that it might be the planet's Bondi sphere. For illustration purposes, the time evolution of the mass inside the planet's Hill radius is shown in Fig. 8 for three gravitoturbulent runs with  $\beta = 30$ . It is comparable to, albeit somewhat larger than the planet mass. It progressively grows as the planet moves inwards, despite the decrease in the planet's Hill radius with decreasing orbital separation. It is possible that the short cooling timescales used in our simple cooling prescription (a few dynamical timescales, depending on  $\beta$ ) implies that the gas in the planet's Hill radius can contract more rapidly than it would do with a more realistic cooling function. Again, notwithstanding the uncertain dynamical role of the planet's Hill sphere in turbulent disc models, it is likely that the increased effective mass is responsible for an increase in the migration rate by a factor of a few compared to laminar calculations (which only include the axisymmetric component of the disc's self-gravity). We comment that both the increase in the effective planet mass, and the decrease in the disc aspect ratio with radius (in discs with flat temperature profile,  $h \propto r^{1/2}$ ), make planets less and less sensitive to stochastic kicks as they migrate inwards. This explains why in Fig. 5 the amplitude of the stochastic kicks decreases with decreasing orbital separation. This also implies that, if a planet undergoes a vigorous inward kick, it will be increasingly harder to reverse the trend. However, should a planet experience a large outward kick, it would take longer for the tidal torque to take over and lead to inward migration again.

### 3.2.4 Impact of numerics

We briefly assess in this section the impact of numerics on our results of gravitoturbulent calculations. We have performed an additional suite of simulations with the Jupiter-mass planet and  $\beta = 30$ , with the planet's mass first smoothly ramped up over one orbit, while the planet is held on a Keplerian orbit. After this, the planet is released in the disc. This procedure is meant to mimic the clump formation, which typically occurs over a dynamical timescale, much shorter than the gap-opening timescale (see Section 3.2.3). The time evolution of the planet's orbital separation is depicted in the left panel of Fig. 9. It shows the very same trend as obtained without smoothly increasing the planet's mass (see the mid-bottom panel of Fig. 4).

To assess the influence of resolution on our simulation results, we have varied the grid's resolution, and the softening length  $\varepsilon_{\text{sg}}$  over which the self-gravitating acceleration is smoothed. We have run two additional disc models with  $\beta = 30$ , one with an increased grid resolution ( $1024 \times 2048$ ), and one with a larger  $\varepsilon_{\text{sg}}$  ( $3 \times 10^{-2} r$ ). In the latter case,  $\varepsilon_{\text{sg}}$  is 0.3 times the initial pressure scale height, and it can be regarded as a crude treatment for the effects of the disc's finite thickness. The value of  $\varepsilon_{\text{sg}}$  at  $r = r_p$  equals the softening length of the planet's gravitational potential. We have checked that before the introduction of the planet at 30 orbits the disc properties (density and temperature profiles) in both additional models are in close agreement with those of the corresponding run at our fiducial resolution and softening length value. We restarted these simulations with a Jupiter-mass planet. Again, in each case, a series of eight simulations was performed with evenly-spaced values for the planet's azimuth at restart. Results with increased grid resolution, and increased  $\varepsilon_{\text{sg}}$  are depicted in the middle and right panels of Fig. 9, respectively. Overall, the amplitude of the stochastic fluctuations is somewhat larger in the high-resolution simulations. Still, except in one run that features a rather long episode of outward

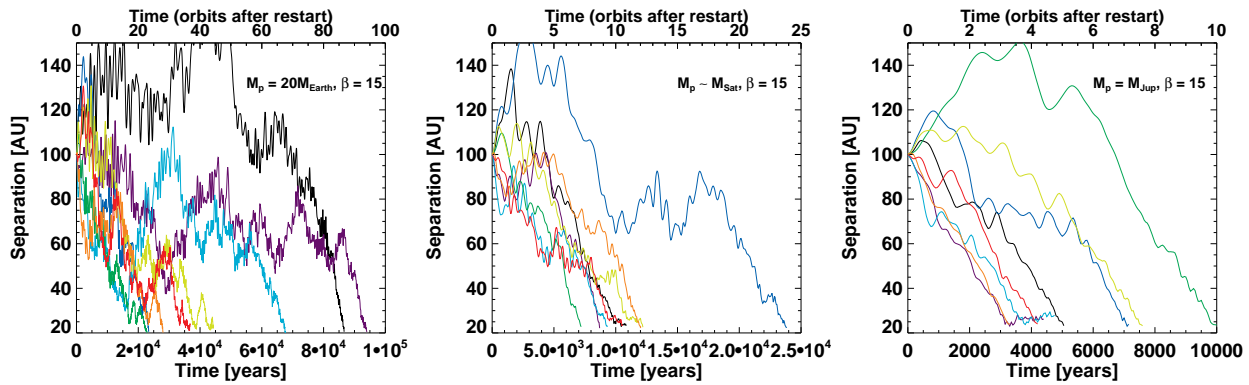


**Figure 10.** Time evolution of the planets’ orbital separation for the disc model with  $\beta = 15$  restarted at 85 orbits, when the disc aspect ratio is  $\approx 6\%$ . From left to right, results are shown for a 20 Earth-mass planet ( $q = 6 \times 10^{-5}$ ,  $q/h_p^3 \sim 0.3$ ), a  $\sim$  Saturn-mass planet ( $q = 2 \times 10^{-4}$ ,  $q/h_p^3 \sim 1.5$ ), and a Jupiter-mass planet ( $q = 10^{-3}$ ,  $q/h_p^3 \sim 5$ ). As in the previous figures, results are obtained for eight evenly-spaced planet’s azimuths at restart (increasing with increasing wavelength’s color).

migration, the migration timescale of the high-resolution simulations ranges from about 3 to 9 orbits, which is broadly consistent with the results at our fiducial resolution. Furthermore, increasing  $\varepsilon_{\text{sg}}$  from  $3 \times 10^{-4} r$  to  $3 \times 10^{-2} r$  does not significantly change the amplitude of the stochastic kicks experienced by the planet, and the migration timescales obtained with both values of  $\varepsilon_{\text{sg}}$  are in reasonable agreement. The results of both additional disc models indicate that the planet’s orbital evolution is essentially unaltered by density structures arising from gravitoturbulence with typical size  $\lesssim 0.3H$ .

### 3.3 Results at lower disc temperature

As shown in Section 3.2, the migration of planets formed by gravitational instability results from a competition between the background disc–planet tidal torque, and the stochastic torque due to turbulence. At least in the early stages of their evolution, such planets should have a planet-to-primary mass ratio  $q \sim h_p^3$ , and be subject to type I-like migration (see Section 3.2.3). As far as the tidal torque is concerned, Eq. (7) shows that the migration timescale is essentially controlled by three dimensionless parameters:  $q/h_p^3$ , which should be  $\sim 1$  in the early stages of the planet evolution,  $Q_p$ , which is  $\gtrsim 1.5$  in a steady state, and  $h_p$ . The disc model that we have considered so far has  $h_p \sim 0.1$ , which leads to rapidly formed Jupiter-mass planets. However, it is possible that the disc initially has a lower aspect ratio, thereby forming less massive planets. The latter may still become Jupiter-sized objects if mass growth is efficient.

To evaluate the impact of a lower disc temperature on our results, we restarted the simulation of Section 3.1 with  $\beta = 15$  at 85 orbits. At this time, the disc aspect ratio at the planet’s restart location (100 AU) has decreased from 0.1 to about 0.06, and the disc’s mass from  $0.2M_\star$  to  $0.15M_\star$ . We choose again three planet masses corresponding to a planet-to-primary ratio  $q$  around  $h_p^3$ : a 20 Earth-mass planet ( $q = 6 \times 10^{-5}$ ,  $q/h_p^3 \sim 0.3$ ), a  $\sim$  Saturn-mass planet ( $q = 2 \times 10^{-4}$ ,  $q/h_p^3 \sim 1$ ), and a Jupiter-mass planet ( $q = 10^{-3}$ ,  $q/h_p^3 \sim 5$ ). As previously,

we take eight evenly-spaced planet’s azimuths at restart. The time evolution of the planets’ orbital separation is shown in Fig. 10.

Compared to the results with  $h_p = 0.1$ , planets with the same  $q/h_p^3$  are now more sensitive to stochastic fluctuations, the tidal torque becoming less vigorous. This can be seen from Eq. (7), which indicates that at fixed values of  $q/h_p^3$  and  $Q_p$ , the migration timescale due to the tidal torque scales with  $h_p^{-2}$ . The mean migration timescales that we obtain for  $h_p \sim 0.06$  (about 6, 12, and 50 orbits with decreasing  $q/h_p^3$ ) are typically a factor of 3–5 longer than in the corresponding runs with  $h_p \sim 0.1$ , which is roughly consistent with the aforementioned scaling  $\tau_I \propto h_p^{-2}$ .

## 4 CONCLUDING REMARKS

Planets observed at large orbital separation from their host star (typically  $\gtrsim 50$  AU) are thought to be potential candidates for the formation scenario based on the gravitational instability of massive discs. A number of studies have shown that the formation of clumps by fragmentation is possible at such separations (e.g., Rafikov 2005; Matzner & Levin 2005; Stamatellos & Whitworth 2008). The orbital evolution of clumps formed by gravitational instability has been investigated in a few studies (e.g., Mayer et al. 2002; Boss 2005; Vorobyov & Basu 2010a; Cha & Nayakshin 2010; Machida et al. 2011). Clumps are often observed to migrate inwards on short timescales, although in some disc models the formation of several clumps and/or the use of different cooling functions has a significant impact on migration, which sometimes appears to be suppressed (Boss 2005).

In this paper, we have studied the interaction between a single planet and the gravitoturbulent disc it is embedded in, following the assumption that the planet has formed by gravitational instability. We have performed 2D hydrodynamical simulations with a simplified prescription for the disc’s cooling. Three disc models with different cooling timescales have been considered, giving rise to different levels of gravitoturbulence. After having

set up a quasi-steady state gravitoturbulent disc, we have restarted our simulations including a single planet with a range of masses approximately equal to the expected initial mass of clumps formed by fragmentation ( $\gtrsim h^3 M_*$ , with  $h$  the disc aspect ratio at the fragmenting location; see Boley et al. 2010).

We find that a planet interacting with its nascent gravitoturbulent disc migrates inwards on very short timescales, despite the stochastic kicks due to turbulent density fluctuations. In a disc with aspect ratio  $\sim 0.1$ , it takes less than 10 orbits at 100 AU (that is, about  $10^4$  years) for a Jupiter-mass planet to migrate from 100 AU to 20 AU (the inner edge of our computational grid). Planets less massive than the expected fragmenting mass are more sensitive to stochastic kicks, but also migrate inwards relatively fast. Their formation and migration timescales being shorter than their gap-opening timescale (partly because of the disc's vigorous turbulence), planets formed by fragmentation do not open a dip or a gap around their orbit, and are therefore not subject to the type II and runaway type III migration regimes. Turbulent density fluctuations may provide an effective mass deficit in the planet's horseshoe region that kicks the planet either inwards or outwards (see Section 3.2.2). These kicks can be seen as an effective, *temporary* type III migration coming on top of the inward migration due to the background disc-planet tidal torque.

The comparison of our results with those of laminar disc models shows that the averaged tidal torque driving the net inward migration in gravitoturbulent discs is essentially the one that would lead to type I migration in the absence of turbulence (see Section 3.2.3). Part of the reason as to why planets rapidly migrate inwards in our model is due to the set up of a positive entropy gradient in a steady state, which yields a large negative horseshoe drag, adding up to the negative differential Lindblad torque. We argue that in gravitoturbulent discs with uniform Toomre- $Q$  profiles and cooling-to-orbital timescale ratios (that is, with a uniform alpha parameter), the horseshoe drag should be negative, unless the surface density decreases very steeply (see Eq. 4). Although this possibility cannot be excluded, we believe that fast inward migration should be a generic expectation for planets formed by gravitational instability.

The main conclusion of this present study is that a single planet formed by gravitational instability should migrate inwards on a timescale much shorter than the expected lifetime of protoplanetary discs. However, it is not possible at this stage to say that massive planets at large separation from their host star, such as the HR 8799 system, *could not* have formed by gravitational instability. The simulations presented here contain a number of simplifications that need to be addressed. We have considered a simplified cooling prescription, causing the entire disc to be gravitoturbulent. In reality, we would expect the inner parts of a disc to be too hot to be gravitationally unstable, and other sources of turbulence such as the magnetorotational instability could prevail (see e.g., Zhu et al. 2009; Rice & Armitage 2009; Clarke 2009, who studied the radial dependence of the alpha viscosity parameter in self-gravitating discs with realistic cooling). It is thus possible that the rapid type I migration of planets

formed by gravitational instability gets slowed down in the disc inner parts, resulting in gap formation. A more realistic cooling prescription will also impact the rate at which planets can contract, with various outcomes for the evolution of the planet mass over its orbital migration (e.g., Nayakshin 2010). Also, we have focused on the orbital evolution of a single planet assumed to have formed by fragmentation, whereas the formation of multiple clumps is a likely outcome of gravitational instability. It is fully expected that the interaction between clumps may significantly impact their migration. We will address these issues in future work.

## APPENDIX A: CALCULATION OF THE ALPHA PARAMETERS IN A TWO-DIMENSIONAL DISC

When mass is confined to a razor-thin disc, the calculation of the alpha parameters associated with the Reynolds and gravitational stresses may be inferred from the general three-dimensional case by substituting the volume mass density  $\rho$  with  $\Sigma\delta(z)$ , where  $\Sigma$  is the surface mass density of the razor-thin disc,  $\delta$  is Dirac's delta function, and  $z$  denotes the vertical coordinate. One obtains (Lynden-Bell & Kalnajs 1972; Gammie 2001)

$$\alpha_{\text{Rey}} = \frac{2}{3} \frac{\langle \Sigma \delta v_r \delta v_\varphi \rangle}{\langle \Sigma c_s^2 \rangle}, \quad (\text{A1})$$

where  $\langle \cdot \rangle$  stands for the azimuthal average,  $\delta v_r = v_r - \langle v_r \rangle$ ,  $\delta v_\varphi = v_\varphi - \langle v_\varphi \rangle$ , and

$$\alpha_{\text{sg}} = \frac{2}{3} \frac{\langle \int_{-\infty}^{\infty} (4\pi G)^{-1} g_r g_\varphi dz \rangle}{\langle \Sigma c_s^2 \rangle}. \quad (\text{A2})$$

In both previous equations,  $v_r$ ,  $v_\varphi$  and  $c_s$  are to be evaluated in the razor-thin disc ( $z \equiv 0$ ) and are therefore directly computed in a 2D simulation. However, the vertical dependence of  $g_r$  and  $g_\varphi$ , the radial and azimuthal components of the self-gravitating acceleration, needs to be determined as the gravitational field outside the disc contributes to the shear stress despite mass being confined to the disc. The potential  $\Phi$  from which  $g_r$  and  $g_\varphi$  can be derived is given by

$$\Phi = - \int_{\mathcal{D}} \frac{G \Sigma(r', \varphi') r' dr' d\varphi'}{\sqrt{r^2 + r'^2 - 2rr' \cos(\varphi - \varphi') + z^2 + \varepsilon_{\text{sg}}^2}} \quad (\text{A3})$$

where  $\mathcal{D}$  is the domain where  $\Sigma$  does not vanish, and  $\varepsilon_{\text{sg}}$  is a small softening length required to avoid numerical divergences when  $z = 0$ . From the surface density of our 2D simulations,  $g_r(r, \varphi, z)$  and  $g_\varphi(r, \varphi, z)$  can be conveniently calculated by fast Fourier transforms provided that  $z$  is taken proportional to  $r$ , condition required for  $g_r$  and  $g_\varphi$  to read as convolution products (another necessary condition is that a grid with logarithmic radial spacing is used). The same condition applies to  $\varepsilon_{\text{sg}}$  for the calculation of  $g_r$  and  $g_\varphi$  at  $z = 0$ . Writing  $\varepsilon_{\text{sg}} = Br$  and  $z = \eta r$ , with  $B$  and  $\eta$  constants, the expressions for  $g_r(r, \varphi, z)$  and  $g_\varphi(r, \varphi, z)$  are given by Eqs. (A1) and (A3) of Baruteau & Masset (2008b) with  $B^2 \rightarrow B^2 + \eta^2$ . The vertical integral in Eq. (A2) is then numerically calculated from the values of  $g_r$  and  $g_\varphi$  obtained with a range of values for  $\eta$ .

## ACKNOWLEDGMENTS

CB is supported by a Herchel Smith Postdoctoral Fellowship. FM is grateful for funding from the EC Sixth Framework Programme and also acknowledges the support of the German Research Foundation (DFG) through grant KL 650/8-2 within the Collaborative Research Group FOR 759: *The formation of Planets: The Critical First Growth Phase*. SJP is supported by an STFC Postdoctoral Fellowship. Numerical simulations were performed on the Pleiades and Grape clusters at U.C. Santa Cruz. Part of this project was done during the 2010 edition of the ISIMA summer school, whose support is gratefully acknowledged. We thank John Papaloizou and Andrew Youdin for useful discussions, Min-Kai Lin for detailed comments on a first draft of this manuscript, and the referee for useful comments.

## REFERENCES

- Balbus S. A., Papaloizou J. C. B., 1999, *ApJ*, 521, 650  
 Baruteau C., Lin D. N. C., 2010, *ApJ*, 709, 759  
 Baruteau C., Masset F., 2008a, *ApJ*, 672, 1054  
 Baruteau C., Masset F., 2008b, *ApJ*, 678, 483  
 Boley A. C., Hayfield T., Mayer L., Durisen R. H., 2010, *Icarus*, 207, 509  
 Boss A. P., 1997, *Science*, 276, 1836  
 Boss A. P., 2005, *ApJ*, 629, 535  
 Bryden G., Różyczka M., Lin D. N. C., Bodenheimer P., 2000, *ApJ*, 540, 1091  
 Cameron A. G. W., 1978, *Moon and Planets*, 18, 5  
 Cha S., Nayakshin S., 2010, *ArXiv e-prints*  
 Clarke C. J., 2009, *MNRAS*, 396, 1066  
 Cossins P., Lodato G., Clarke C. J., 2009, *MNRAS*, 393, 1157  
 Crida A., Baruteau C., Kley W., Masset F., 2009, *A&A*, 502, 679  
 Crida A., Masset F., Morbidelli A., 2009, *ApJL*, 705, L148  
 Crida A., Morbidelli A., Masset F., 2006, *Icarus*, 181, 587  
 Gammie C. F., 2001, *ApJ*, 553, 174  
 Goldreich P., Tremaine S., 1980, *ApJ*, 241, 425  
 Helled R., Bodenheimer P., 2011, *Icarus*, 211, 939  
 Ida S., Lin D. N. C., 2004, *ApJ*, 604, 388  
 Ida S., Lin D. N. C., 2008, *ApJ*, 673, 487  
 Kalas P., Graham J. R., Chiang E., Fitzgerald M. P., Clampin M., Kite E. S., Stapelfeldt K., Marois C., Krist J., 2008, *Science*, 322, 1345  
 Lafrenière D., Jayawardhana R., van Kerkwijk M. H., 2010, *ApJ*, 719, 497  
 Lagrange A., Bonnefoy M., Chauvin G., Apai D., Ehrenreich D., Boccaletti A., Gratadour D., Rouan D., Mouillet D., Lacour S., Kasper M., 2010, *Science*, 329, 57  
 Lin M.-K., Papaloizou J. C. B., 2010, *MNRAS*, 405, 1473  
 Lodato G., Rice W. K. M., 2004, *MNRAS*, 351, 630  
 Lynden-Bell D., Kalnajs A. J., 1972, *MNRAS*, 157, 1  
 Machida M. N., Inutsuka S., Matsumoto T., 2011, *ApJ*, 729, 42  
 Marois C., Macintosh B., Barman T., Zuckerman B., Song I., Patience J., Lafrenière D., Doyon R., 2008, *Science*, 322, 1348  
 Marois C., Zuckerman B., Konopacky Q. M., Macintosh B., Barman T., 2010, *Nature*, 468, 1080  
 Masset F., 2000, *A&AS*, 141, 165  
 Masset F. S., 2002, *A&A*, 387, 605  
 Masset F. S., Casoli J., 2009, *ApJ*, 703, 857  
 Masset F. S., Casoli J., 2010, *ApJ*, 723, 1393  
 Masset F. S., D'Angelo G., Kley W., 2006, *ApJ*, 652, 730  
 Masset F. S., Papaloizou J. C. B., 2003, *ApJ*, 588, 494  
 Matzner C. D., Levin Y., 2005, *ApJ*, 628, 817  
 Mayer L., Quinn T., Wadsley J., Stadel J., 2002, *Science*, 298, 1756  
 Meru F., Bate M. R., 2011a, *MNRAS*, 411, L1  
 Meru F., Bate M. R., 2011b, *MNRAS*, 410, 559  
 Mizuno H., 1980, *Progress of Theoretical Physics*, 64, 544  
 Nayakshin S., 2010, *MNRAS*, 408, L36  
 Nelson R. P., Papaloizou J. C. B., 2004, *MNRAS*, 350, 849  
 Paardekooper S., Baruteau C., Crida A., Kley W., 2010, *MNRAS*, 401, 1950  
 Paardekooper S., Baruteau C., Kley W., 2011, *MNRAS*, 410, 293  
 Paardekooper S.-J., Baruteau C., Meru F., 2011, *MNRAS*, submitted  
 Paardekooper S.-J., Papaloizou J. C. B., 2008, *A&A*, 485, 877  
 Paardekooper S.-J., Papaloizou J. C. B., 2009, *MNRAS*, 394, 2283  
 Pierens A., Hüré J.-M., 2005, *A&A*, 433, L37  
 Pollack J. B., Hubickyj O., Bodenheimer P., Lissauer J. J., Podolak M., Greenzweig Y., 1996, *Icarus*, 124, 62  
 Rafikov R. R., 2005, *ApJL*, 621, L69  
 Rice W. K. M., Armitage P. J., 2009, *MNRAS*, 396, 2228  
 Rice W. K. M., Lodato G., Armitage P. J., 2005, *MNRAS*, 364, L56  
 Safronov V. S., 1969, *Evoliutsiia doplanetnogo oblaka.. Moscow: Nauka*  
 Stamatellos D., Whitworth A. P., 2008, *A&A*, 480, 879  
 Stone J. M., Norman M. L., 1992, *ApJS*, 80, 753  
 Thommes E. W., 2005, *ApJ*, 626, 1033  
 Toomre A., 1964, *ApJ*, 139, 1217  
 Vorobyov E. I., Basu S., 2006, *ApJ*, 650, 956  
 Vorobyov E. I., Basu S., 2010a, *ApJL*, 714, L133  
 Vorobyov E. I., Basu S., 2010b, *ApJ*, 719, 1896  
 Zhu Z., Hartmann L., Gammie C., 2009, *ApJ*, 694, 1045